



Spatial structure of the pair wave function and the density correlation functions throughout the BEC-BCS crossover

J. C. Obeso-Jureidini and V. Romero-Rochín 
*Instituto de Física, Universidad Nacional Autónoma de México
 and Apartado Postal 20-364, 01000 Cd. México, Mexico*

 (Received 24 October 2019; revised manuscript received 25 February 2020; accepted 26 February 2020; published 27 March 2020)

Within the BCS-Leggett mean-field model of a balanced mixture of two different spin fermionic atoms, we calculate the BCS pair probability distribution and the density correlation functions both between atoms with the same and different spin states, being able to accurately extract their spatial large-distance behavior along the BEC-BCS crossover. It is found that, after different initial transients, these distributions show an exponential decay and a well-defined periodic oscillatory behavior, which we analyze throughout the whole crossover. In addition, we derive analytic expressions for the mean pair size and the correlation lengths of the same and different density correlation functions. While in general, in the BCS side, there are long-range correlations and, in the BEC region, the behavior is dominated by tight-pair formation, each distribution shows its own characteristic behavior, yielding all together a quite complete description of the spatial structure of the superfluid along the crossover.

DOI: [10.1103/PhysRevA.101.033619](https://doi.org/10.1103/PhysRevA.101.033619)

I. INTRODUCTION

The physics of a mixture of two fermionic species with tunable interactions remains as a subject of current interest. Such a model system is ubiquitous in a wide range of physical phenomena, ranging from its realization in ultracold gases, commonly found now in many laboratories [1–10] as one explanation of high-temperature superconductivity [11–15], to a description of nuclear matter in certain stars [16–20]. The overall physical picture is of a gas of large, overlapping Cooper pairs of atoms in the Bardeen-Cooper-Schrieffer (BCS) regime and, in the other extreme, a Bose-Einstein condensate (BEC) of tight molecules, with a smooth crossover occurring in the neighborhood within the two-body collision scattering resonance and the sign change of the chemical potential [21–24]. The theoretical work on this subject is already overwhelming; for instance, see Refs. [16,25,26] as excellent reviews. An important and apparently simple question concerns the size of the pairs of atoms of the two different species along the crossover and, although there are already several discussions to answer this question [15,25,27–32], it does not and perhaps cannot have a simple or sole answer since this is clearly a many-body problem. Here, we readdress this question and pose it more as an analysis of the spatial structure of the mixture rather than just a question concerning the size of the pairs. For this goal, within the mean-field BCS-Leggett theory, by an accurate calculation of their spatial dependence, we study the following two-body distributions: the BCS pair wave function, the density correlation function of atoms of different species and the density correlation function of like particles. The three of them are obtained directly from the standard variational solution of the problem at zero temperature [23]. In addition, we introduce a postulated “pair-binding” wave function or distribution, based

on the pair-binding energy [33], as a reference for the previous three functions.

Our analysis is based mainly on a numerical evaluation of the spatial dependence for the mentioned distributions, which allows us to accurately fit their exponential decay length as well as their oscillatory wave numbers and phases for long distances. In addition, we provide exact analytical expressions for the correlation lengths of all the distributions, being defined as the normalized second moment of each distribution [16]. These characteristic lengths and the associated oscillatory behavior yield a very complete picture of the physical nature of the pairing phenomenon along the whole crossover. We first observe that the three distribution functions behave differently in some regions while similarly in others. For instance, on the BCS side, both correlation functions, of the same and different species, show the expected long-range behavior with divergent coherence or correlation lengths, while the BCS probability distribution shows a finite average pair radius [27]. The three previous results put together indicate that, in the BCS limit, although the pair mean size is finite there are pairs of all sizes as all distributions decay algebraically. On the other limit, at BEC, now the unlike particle correlation function and the BCS pair probability distribution have the same localized behavior, while the same species correlation function decays extremely fast in its own way. This is certainly another indication of the formation of a gas of bosonic molecules where there are no Pauli-blocking correlations of atoms in the same spin state. The binding-pair distribution is a reference that fits quite well the envelope of the calculated distributions in the crossover. Regarding the oscillatory behavior, we find that, in the long-distance limit, the three distributions spatially oscillate with the same wave number that tends to the Fermi momentum in the BCS limit

and vanishes in the BEC limit. The like and unlike atomic correlations oscillate perfectly out of phase, showing a nested structure that becomes more evident in the BCS limit. While such a structure remains in the BEC side, it is evidently arrested by the fast exponential decay and low-frequency oscillations. The BCS wave function oscillates with the same frequency but its relative phase changes along the crossover.

The article is organized as follows: First we briefly review the BCS-Leggett mean-field model as a reference for the calculation and discussion of the pair BCS wave function and the correlation functions in the following sections. In Sec. III we discuss the mentioned distributions and discuss how, by deforming the Fourier transform contours in the k complex plane, we are able to calculate numerically the distributions for any pair spatial separation. In Sec. IV we analyze the average pair radius and the correlation lengths by means of exact analytical expressions. We conclude with some final remarks. In the Appendix we give the essential details for the contour deformation of Sec. III and the exact analytical expressions that we provide along in the text.

II. BEC-BCS MEAN-FIELD CONTACT INTERACTION MIXTURE GAS

We consider the usual contact-interaction many-body Hamiltonian of a balanced gas mixture of fermion atoms in two hyperfine states $\sigma = \uparrow, \downarrow$ in the low-density and low-energy regime, using the grand potential $\hat{\Omega} = \hat{H} - \mu\hat{N}$,

$$\hat{\Omega} = \sum_{\mathbf{k}, \sigma} (\epsilon_{\mathbf{k}} - \mu) c_{\mathbf{k}\sigma}^\dagger c_{\mathbf{k}\sigma} + \frac{g}{V} \sum_{\mathbf{k}_1} \sum_{\mathbf{k}_4} c_{\mathbf{k}_1\uparrow}^\dagger c_{-\mathbf{k}_1\downarrow}^\dagger c_{-\mathbf{k}_4\downarrow} c_{\mathbf{k}_4\uparrow}, \quad (1)$$

where $g = 4\pi\hbar^2 a/m$ is the interaction constant, a is the s -wave scattering length, $\epsilon_{\mathbf{k}} = \hbar^2 k^2/2m$, V is the volume of the sample, and the sums are over all wave vectors \mathbf{k} . To find the ground state we use the BCS-Leggett variational method [22,23,34], although one can also rely on the mean-field method [16], or the exact solution in the thermodynamic limit [27]. The BCS-Leggett variational approach introduces the BCS wave function to minimize the grand potential

$$|\Psi_{\text{BCS}}\rangle = \prod_{\mathbf{k}} (u_{\mathbf{k}} + v_{\mathbf{k}} c_{\mathbf{k}\uparrow}^\dagger c_{-\mathbf{k}\downarrow}^\dagger) |0\rangle, \quad (2)$$

where $\hat{c}_{\mathbf{k}\sigma}^\dagger$ are the creation operators of fermionic atoms with momentum \mathbf{k} and spin $\sigma = \uparrow, \downarrow$. The variational parameters satisfy the normalization condition $|u_{\mathbf{k}}|^2 + |v_{\mathbf{k}}|^2 = 1$ and are given by

$$\begin{cases} u_{\mathbf{k}}^2 \\ v_{\mathbf{k}}^2 \end{cases} = \frac{1}{2} \left[1 \pm \frac{\epsilon_{\mathbf{k}} - \mu}{\sqrt{(\epsilon_{\mathbf{k}} - \mu)^2 + \Delta^2}} \right], \quad (3)$$

where the gap Δ has been introduced. For completeness and for further purposes below, we first give analytic expressions for the thermodynamic variables: the regularized gap Δ , the number $N = \langle \hat{N} \rangle$, and the gas ground-state energy $E_0 = \langle \hat{H} \rangle$ equations. As shown in the Appendix, these quantities and the second moments of the distributions, defined below, can all be expressed in terms of hypergeometric functions $F = {}_2F_1(a, b; c, (1-z)/2)$, which in some cases can also be expressed in terms of Legendre functions $P_\mu^{\nu}(z)$, with z being a

natural dimensionless quantity,

$$z = -\frac{\mu}{\sqrt{\mu^2 + \Delta^2}}. \quad (4)$$

We note that $-1 < z < +1$, and that the deep BCS limit, $a \rightarrow 0^-$, is $z \rightarrow -1$, while the BEC limit, $a \rightarrow 0^+$, is $z \rightarrow +1$. In all the expressions we use the thermodynamic limit $\sum_{\mathbf{k}} \rightarrow \frac{V}{(2\pi)^3} \int d^3k$. Then, the so-called regularized gap equation, which expresses the scattering length a in terms of the chemical potential μ and the gap Δ , can be written as

$$-\frac{m}{4\pi\hbar^2 a} = \frac{1}{2V} \sum_{\mathbf{k}} \left(\frac{1}{\sqrt{(\epsilon_{\mathbf{k}} - \mu)^2 + \Delta^2}} - \frac{1}{\epsilon_{\mathbf{k}}} \right) = -\frac{1}{8\pi} \left(\frac{2m}{\hbar^2} \right)^{3/2} (\mu^2 + \Delta^2)^{1/4} P_{\frac{1}{2}}(z), \quad (5)$$

while the number, or rather the particle density equation, $n = N/V$, is

$$n = \frac{1}{V} \sum_{\mathbf{k}} \left(1 - \frac{\epsilon_{\mathbf{k}} - \mu}{\sqrt{(\epsilon_{\mathbf{k}} - \mu)^2 + \Delta^2}} \right) = \frac{1}{4\pi} \left(\frac{2m}{\hbar^2} \right)^{3/2} (\mu^2 + \Delta^2)^{3/4} [-P_{\frac{3}{2}}(z) + zP_{\frac{1}{2}}(z)]. \quad (6)$$

Since we are considering a balanced mixture, the number of \uparrow atoms equal those of spin \downarrow , being $N/2$.

In the same way, the total energy density $e_0 = E_0/V$ is

$$e_0 = \frac{1}{V} \sum_{\mathbf{k}} \left(\epsilon_{\mathbf{k}} - \frac{\epsilon_{\mathbf{k}}(\epsilon_{\mathbf{k}} - \mu) - \Delta^2/2}{\sqrt{(\epsilon_{\mathbf{k}} - \mu)^2 + \Delta^2}} \right) = \frac{1}{4\pi} \left(\frac{2m}{\hbar^2} \right)^{3/2} (\mu^2 + \Delta^2)^{5/4} \times \left[P_{\frac{5}{2}}(z) - zP_{\frac{3}{2}}(z) + \frac{1}{2}(1-z^2)P_{\frac{1}{2}}(z) \right]. \quad (7)$$

The above quantities have already been found in similar or other forms in other references [27–29]. We do include them here for the analysis performed below.

Combining Eqs. (5) and (6) into Eq. (7), and using a recursion relation of Legendre functions, yields the following closed expression of e_0 in terms of the four thermodynamic quantities n , μ , a , and Δ ,

$$e_0 = -\frac{1}{5} \left[\frac{m}{4\pi\hbar^2 a} \Delta^2 - 3\mu n \right]. \quad (8)$$

As it will be of use below, we can identify the binding energy per pair as [27]

$$\epsilon_b = \frac{2}{N} (E_F - E_0) = \frac{2}{5n} \left[3(\epsilon_F - \mu)n + \frac{m}{4\pi\hbar^2 a} \Delta^2 \right], \quad (9)$$

where $E_F = (3/5)N\epsilon_F$ is the ground-state energy of N free fermions, with $\epsilon_F = \hbar^2 k_F^2/2m$ and $k_F = (3\pi^2 n)^{1/3}$ being the Fermi energy and momentum of the free gas, respectively. In the mean-field method the quasiparticle spectrum suggests that the energy to create such an excitation with $k \approx 0$ is given by

$$\epsilon_{\text{spec}} = \sqrt{\mu^2 + \Delta^2} - \mu. \quad (10)$$

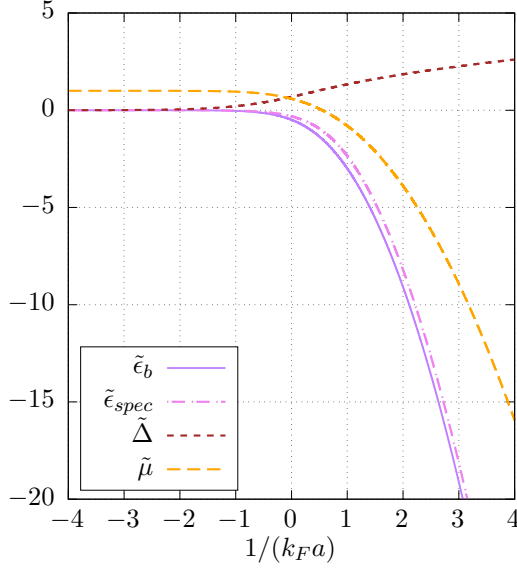


FIG. 1. Dimensionless chemical potential $\tilde{\mu} = \mu/\epsilon_F$, gap $\tilde{\Delta} = \Delta/\epsilon_F$, binding-pair energy $\tilde{\epsilon}_b = \epsilon_b/\epsilon_F$, and spectroscopic threshold $\tilde{\epsilon}_{\text{spec}} = \epsilon_{\text{spec}}/\epsilon_F$, as functions of $1/k_F a$.

This quantity has been used to analyze rf-spectroscopy of pair dissociation [25,35]. As we see below, this energy is very close to ϵ_b along the whole crossover.

As discussed in many texts, Eqs. (5) and (6) can be used to solve for Δ and μ as functions of n and a , thus allowing us to express all the physical quantities of the crossover in terms of the latter as the independent thermodynamic variables. As shown since the work of Leggett [23], the dependence of all physical quantities on n and a can be expressed in terms of the Fermi energy ϵ_F and the dimensionless quantity $1/k_F a$. Hence, in Fig. 1 we plot μ , Δ , ϵ_b , and ϵ_{spec} , scaled with ϵ_F , as functions of $1/k_F a$. The behavior of Δ and μ is already well known, showing the relevance of the gap Δ over the chemical potential μ on the BCS side, while the opposite happens in the BEC extreme. It is interesting to observe that both ϵ_b and ϵ_{spec} behave similarly as the gap on the BCS side and to the chemical potential in the BEC limit, thus serving as interpolations between the two limits. As we see below, the opposite spin-correlation length is closely related to these two energies. Also, as obtained from the previous equations, see also Ref. [27], we quote here the asymptotic values of Δ , μ , and ϵ_b in the BCS and BEC limits, $1/k_F a \rightarrow -\infty$ and $1/k_F a \rightarrow +\infty$, respectively,

$$\begin{aligned} \Delta &\approx 8\epsilon_F e^{-2} e^{\frac{\pi}{2k_F a}}, & \mu &\approx \epsilon_F \left(1 + 8e^{-4} \left[\frac{\pi}{k_F a} - 5 \right] \right) e^{\frac{\pi}{k_F a}}, \\ \epsilon_b &\approx 48\epsilon_F e^{-4} e^{\frac{\pi}{k_F a}} & \text{for } 1/k_F a &\rightarrow -\infty, \\ \Delta &\approx \epsilon_F \left(\frac{16}{3\pi k_F a} \right)^{1/2}, & \mu &\approx -\frac{\epsilon_F}{(k_F a)^2}, \\ \epsilon_b &\approx \frac{2\epsilon_F}{(k_F a)^2} & \text{for } 1/k_F a &\rightarrow +\infty. \end{aligned} \quad (11)$$

From the exact expressions (5) and (6), one can find the known special values, first, at unitarity $1/k_F a = 0$,

$\mu/\epsilon_F \approx 0.59061$, and $\Delta/\epsilon_F \approx 0.68640$; and, second, at $\mu = 0$, $1/k_F a \approx 0.55315$, and $\Delta/\epsilon_F \approx 1.0518$.

III. BCS-PAIR WAVE FUNCTION AND DENSITY CORRELATION FUNCTIONS

As described in the introduction, the spatial structure of the many-body BCS state cannot be solely pinned on a single quantity but, rather, one can look at several relevant quantities that, put together, yield a more complete picture without the need of compromising the concept of what a Cooper pair really is. For this, we look at the three two-body quantities that can be extracted from the variational parameters u_k and v_k . These are the BCS-pair probability density $|\phi_{\text{BCS}}(\mathbf{r})|^2$; the density-density correlation function between different spin species, $G_{\uparrow\downarrow}(\mathbf{r})$; and the density-density correlation function between same species, $G_{\uparrow\uparrow}(\mathbf{r})$. The latter is equal to the $\downarrow\downarrow$ correlation function due to the balance of the mixture. Although these quantities have already been addressed in the literature, the improvement here presented resides on the fact that we are able to accurately calculate their spatial dependence for any distance. In particular, we are able to study the long-range behavior of all of them, yielding not only their *exponential* decay lengths χ_{BCS} , $\chi_{\uparrow\downarrow}$, $\chi_{\uparrow\uparrow}$, but also their respective main oscillatory wavelength or wave number κ_{BCS} , $\kappa_{\uparrow\downarrow}$, $\kappa_{\uparrow\uparrow}$ as well as their relative phases. In addition, as shown in the following section, we also calculate analytically the mean pair radius and the correlation lengths defined as the second moment of the corresponding distributions.

As was already pointed out by Leggett in his seminal work [23], the BCS state, spatially, is the antisymmetric superposition of $\uparrow\downarrow$ pairs, with every pair being in a two-body state given by the following *unnormalized* wave function:

$$\phi_{\text{BCS}}(\mathbf{r}) = \frac{1}{(2\pi)^3} \int d^3\mathbf{k} e^{i\mathbf{k}\cdot\mathbf{r}} \frac{v_{\mathbf{k}}}{u_{\mathbf{k}}}. \quad (12)$$

As it is our claim here, however, the many-body spatial structure also depends on the next-in-importance density correlation functions of like and unlike pairs. To make the appropriate contrast among these three quantities, we stress that, while we calculate the pair wave function, our emphasis is on the BCS pair probability distribution $|\phi_{\text{BCS}}(\mathbf{r})|^2$.

To calculate the density correlation functions we recall that the particle density operator at \mathbf{r} of spin $\sigma = \uparrow$ or \downarrow is given by $\hat{n}_{\sigma}(\mathbf{r}) = \hat{\psi}_{\sigma}^{\dagger}(\mathbf{r})\hat{\psi}_{\sigma}(\mathbf{r})$ with the particle annihilation operator given by

$$\hat{\psi}_{\sigma}(\mathbf{r}) = \frac{1}{\sqrt{V}} \sum_{\mathbf{k}} e^{i\mathbf{k}\cdot\mathbf{r}} \hat{c}_{\mathbf{k},\sigma}. \quad (13)$$

Then, the density correlation function of antiparallel spins $\uparrow\downarrow$ is found to be

$$\begin{aligned} G_{\uparrow\downarrow}(\mathbf{r}, \mathbf{r}') &= \langle \hat{n}_{\uparrow}(\mathbf{r})\hat{n}_{\downarrow}(\mathbf{r}') \rangle - \langle \hat{n}_{\uparrow}(\mathbf{r}) \rangle \langle \hat{n}_{\downarrow}(\mathbf{r}') \rangle \\ &= |g_{\uparrow\downarrow}(\mathbf{r} - \mathbf{r}')|^2, \end{aligned} \quad (14)$$

with $g_{\uparrow\downarrow}(\mathbf{r})$ being the Fourier transform of $v_{\mathbf{k}}u_{\mathbf{k}}$,

$$g_{\uparrow\downarrow}(\mathbf{r}) = \frac{1}{(2\pi)^3} \int d^3\mathbf{k} e^{i\mathbf{k}\cdot\mathbf{r}} v_{\mathbf{k}}u_{\mathbf{k}}. \quad (15)$$

As we discuss further below, this quantity has also been identified as the “pair wave function” in several studies, see Refs. [16,25,31,32]. Here, for definiteness we shall keep it associated with the $\uparrow\downarrow$ density correlations.

Third, the density correlation function with parallel $\uparrow\uparrow$ spins (equal to $\downarrow\downarrow$) can be found to be

$$\begin{aligned} G_{\uparrow\uparrow}(\mathbf{r}, \mathbf{r}') &= \langle \hat{n}_{\uparrow}(\mathbf{r})\hat{n}_{\uparrow}(\mathbf{r}') \rangle - \langle \hat{n}_{\uparrow}(\mathbf{r}) \rangle \langle \hat{n}_{\uparrow}(\mathbf{r}') \rangle \\ &= \frac{n}{2} \delta^3(\mathbf{r} - \mathbf{r}') - |g_{\uparrow\uparrow}(\mathbf{r} - \mathbf{r}')|^2, \end{aligned} \quad (16)$$

where now $g_{\uparrow\uparrow}(\mathbf{r})$ is the Fourier transform of v_k^2 ,

$$g_{\uparrow\uparrow}(\mathbf{r}) = \frac{1}{(2\pi)^3} \int d^3\mathbf{k} e^{i\mathbf{k}\cdot\mathbf{r}} v_k^2. \quad (17)$$

The density correlation function with parallel spins considered here differs from that commonly used in the literature [26,36], the present one including the same site contribution of the spin. This is important to note because the behavior is completely different from those previously used. Hence, at the two-body level, the structure of the BCS state is contained in the quantities v_k/u_k , $u_k v_k$, and v_k^2 . It is of interest to point out that the negative, or anticorrelation, sign in the second term of the equal spin-correlation function reflects the Pauli exclusion principle just as in the ideal Fermi gases [37].

From the previous discussion we see that the evaluation of the BCS-pair probability distribution and of the density correlation functions requires knowledge of $\phi_{\text{BCS}}(\mathbf{r})$, $g_{\uparrow\uparrow}(\mathbf{r})$, and $g_{\uparrow\downarrow}(\mathbf{r})$, which in turn seemingly amounts to performing Fourier transforms, see Eqs. (12), (15), and (17). These three expressions can be generically written as

$$f(\mathbf{r}) = \int d^3\mathbf{k} e^{i\mathbf{k}\cdot\mathbf{r}} \mathcal{F}(\mathbf{k}), \quad (18)$$

with $\mathcal{F}(\mathbf{k})$ being v_k/u_k , $u_k v_k$, and v_k^2 , respectively. Since u_k and v_k depend on $k = |\mathbf{k}|$ only, see Eq. (3), the functions $f(\mathbf{r})$ depends on $r = |\mathbf{r}|$ only as well and, hence, it can be generally written as

$$f(r) = \frac{1}{4\pi^2 i r} \int_{-\infty}^{\infty} e^{ikr} k \mathcal{F}(k) dk. \quad (19)$$

Thus, the task is reduced to perform the one-dimensional Fourier transform of $k\mathcal{F}(k)$. Since $\mathcal{F}(k)$ is a real even function of k , the functions $f(r)$ are also real. Calculating these Fourier transforms numerically may be done by using a common fast Fourier transform code. However, since the functions $\mathcal{F}(k)$ decay algebraically for large k , the numerical precision of $f(r)$ is severely limited, making it very hard to find its large- r behavior. Here we present an alternative approach that allows for an accurate calculation of these Fourier transforms for any value of r , short and very large. This gives rise to very precise fits of the asymptotic forms of the BCS probability distribution and of the density correlation functions yielding a contribution with an exponential decay and an oscillatory component in the long-distance regime, as shown below. The mathematical details are given in the Appendix and here we present just the main aspects of the corresponding calculations.

As usual when dealing with this model, most of the analytical and numerical complications arise from the square root $[(\epsilon_k - \mu)^2 + \Delta^2]^{1/2}$ term and its long- k behavior in the

expressions for u_k and v_k , see Eq. (3). In the k complex plane this square root gives rise to four branch points with their corresponding branch cuts; see the Appendix. Hence, the integral $f(r)$ in Eq. (19) can be extended to the k complex plane, followed by a deformation of the contour integral, thus yielding an alternative expression for $f(r)$ that can be accurately numerically integrated for large values of r . As an example, we write here the expression obtained for the pair wave function $\phi_{\text{BCS}}(r)$ only,

$$\begin{aligned} \phi_{\text{BCS}}(r) &= -\frac{k_F^3}{\pi^2 \tilde{\Delta} k_F r} \int_{\tau_0}^{\infty} \left(\frac{2\tau^2 - \tilde{\mu}}{\sqrt{\tau^2 - \tilde{\mu}}} \right) \\ &\quad \times \sqrt{(2\tau^2 - \tilde{\mu})^2 - (\tilde{\Delta}^2 + \tilde{\mu}^2)} \\ &\quad \times \exp[-\sqrt{\tau^2 - \tilde{\mu}} k_F r] \sin(k_F r \tau) d\tau \end{aligned} \quad (20)$$

where $\tau_0 = \{[\tilde{\mu} + (\tilde{\mu}^2 + \tilde{\Delta}^2)^{1/2}]/2\}^{1/2}$, $\tilde{\mu} = \mu/\epsilon_F$, and $\tilde{\Delta} = \Delta/\epsilon_F$. While the above expression may look complicated, it actually converges very fast and accurately due to the exponentially decaying term in the integrand. The expressions for $g_{\uparrow\uparrow}(\mathbf{r})$ and $g_{\uparrow\downarrow}(\mathbf{r})$ also contain the same exponential term with an analogous fast convergence. Although one can calculate any of the above distributions for any value of r , as shown in Fig. 2, we mainly concentrate on their long-distance behavior, as we now discuss. In the literature these three functions have been studied for short distances [26,36].

A. Exponential decay lengths

The upper panel of Fig. 2 shows the BCS pair probability distribution function $|\phi_{\text{BCS}}(r)|^2$, the $\uparrow\downarrow$ density correlation function $G_{\uparrow\downarrow}(r)$ and the $\uparrow\uparrow$ density correlation function $-G_{\uparrow\uparrow}(r)$ without the δ -function contribution, namely, just the part $|g_{\uparrow\uparrow}(r)|^2$, see Eq. (16), for small values of r , where differences are evident. However, once certain transient has been passed, their asymptotic shape for large values of r appear similar, as can be seen in the corresponding lower panel of Fig. 2. The latter are plots in semilog scale showing an oscillatory behavior with characteristic wave numbers κ_α and phases φ_α , which will be detailed below; here we introduce a subindex to differentiate among the three cases $\alpha = \text{BCS}, \uparrow\downarrow, \uparrow\uparrow$. On top of the oscillations there is a clear exponential decay with a characteristic *exponential decay length* χ_α that certainly depends on $k_F a$. Accurate fits of χ_α , κ_α , and φ_α for each distribution, writing $\rho_\alpha(r) = |\phi_{\text{BCS}}(r)|^2, G_{\uparrow\uparrow}(r), G_{\uparrow\downarrow}(r)$ yields a generic function for the three distributions that can be written as

$$\rho_\alpha(r) \approx \frac{\text{const}}{r^2} e^{-\frac{\sqrt{2}r}{\chi_\alpha}} \mathcal{P}_\alpha(\kappa_\alpha r + \varphi_\alpha), \quad r \gg k_F^{-1}, \quad (21)$$

with $\mathcal{P}_\alpha(\kappa_\alpha r + \varphi_\alpha)$ being a periodic function of r with wavelength $2\pi/\kappa_\alpha$ and phase φ_α . We would like to point out that this full functional form has not been previously studied in all the crossover region for the three functions that we are considering. Indeed, there have been studies at short distances only [25,26,38], where a predominant algebraic behavior is expected. We emphasize here, however, that at long distances there is always an exponential decay.

The previous fit suggests that we associate an additional function that helps to describe the spatial envelope of the pairs.

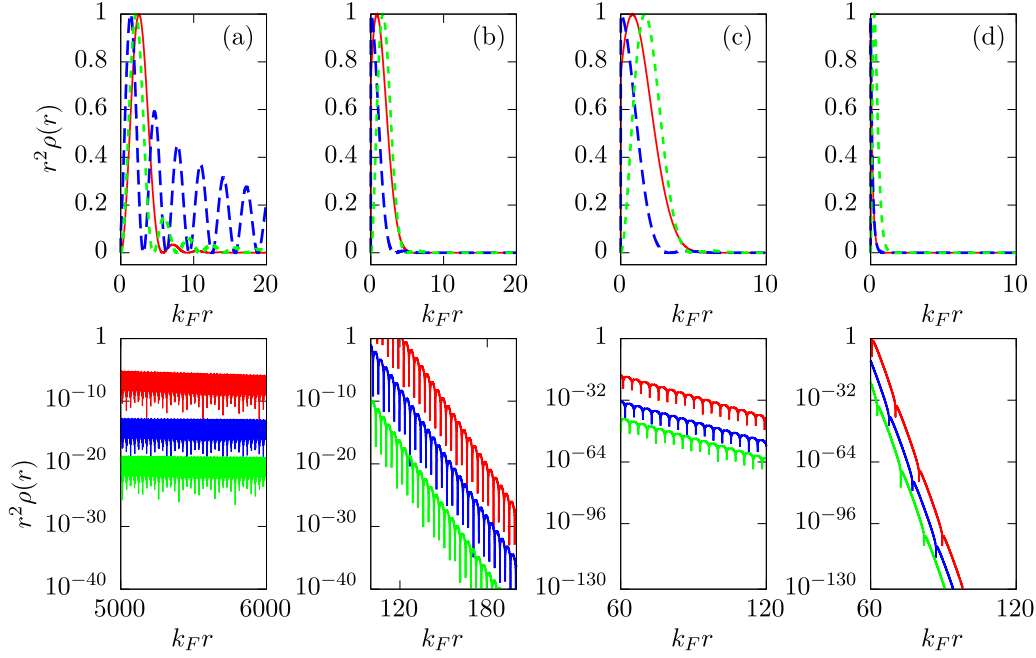


FIG. 2. Distributions $r^2 \rho_\alpha(r)$, with $\rho_\alpha(r) = |\phi_{\text{BCS}}(r)|^2$ (red), $G_{\uparrow\downarrow}(r)$ (green), $G_{\downarrow\uparrow}(r)$ (blue), as functions of $k_F r$, for chosen values of $1/k_F a$ before and after the resonance, (a) $1/k_F a = -5.0$, (b) $1/k_F a = -0.0046$, (c) $1/k_F a = 0.0064$, (d) $1/k_F a = 4.0$. In the upper panel the solid lines correspond to $|\phi_{\text{BCS}}(r)|^2$, long dashed lines to $G_{\uparrow\downarrow}(r)$, and short dashed lines to $-G_{\uparrow\uparrow}(r)$. The lower panel is in semilogarithmic scale. In this panel, the upper curves correspond to $|\phi_{\text{BCS}}(r)|^2$, the middle ones to $G_{\uparrow\downarrow}(r)$, and lower curves to $-G_{\uparrow\uparrow}(r)$. The latter does not include the δ -function contribution in both panels, see Eq. (16).

This we call the *binding-pair* function, which we write as

$$|\Phi_b(r)|^2 = \frac{\text{const}}{r^2} e^{-\sqrt{2}r/\chi_b}, \quad (22)$$

valid for all values of r , with the exponential decay length χ_b given by

$$\chi_b \equiv \left(\frac{\hbar^2}{2m\epsilon_b} \right)^{1/2}, \quad (23)$$

where ϵ_b is the binding energy shown in Eq. (9). A *spectroscopic* length χ_{spec} [25,39] associated with the threshold energy ϵ_{spec} , as given in Eq. (10), can also be used for comparison. In fact, we have found $\chi_{\uparrow\downarrow}$ and $\chi_{\uparrow\uparrow}$ to be well fit by χ_{spec} as well. However, we do not consider it here explicitly since this length is very close to χ_b along the whole crossover, as can be inferred from Fig. 1.

The exponential decay lengths χ_{BCS} , $\chi_{\uparrow\downarrow}$, $\chi_{\uparrow\uparrow}$, and χ_b are plotted as functions of $1/k_F a$ in Fig. 3, the first three with solid lines and the latter with a large dashed line. We note first that in the BEC regime all four exponential decaying lengths behave essentially in the same way, indicating that the dominating length scale is that of χ_b (below we give their analytic asymptotic expression). On the other hand, in the BCS limit, while $\chi_{\uparrow\downarrow}$ and $\chi_{\uparrow\uparrow}$ appear very close to χ_b , χ_{BCS} shows definitely a different behavior, also appearing divergent but at a much slower pace; as we will see below, when we analyze the mean pair size and correlation lengths, also shown in Fig. 3 with dashed lines, this departure makes a profound difference and gives rise to a richer picture of the structure of the mixture gas.

B. Characteristic wave numbers and phases

Two other important spatial features can be extracted from the pair probability density and the correlation functions: these are the characteristic wave number κ_α of the oscillatory function and its phase φ_α . In Fig. 4(a) the plot of κ_{BCS} , $\kappa_{\uparrow\downarrow}$, and $\kappa_{\uparrow\uparrow}$, as functions of $1/k_F a$, shows the striking conclusion that, within our numerical precision, they are exactly the same. This perhaps should not be surprising for the $\uparrow\downarrow$ and $\uparrow\uparrow$

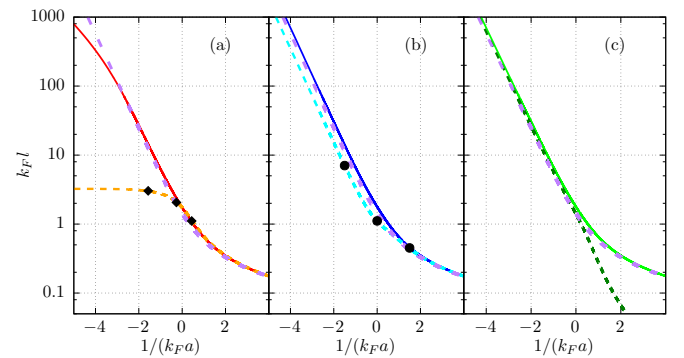


FIG. 3. Exponential decay lengths $l = \chi_\alpha$ and correlation lengths $l = \xi_\alpha$, scaled with k_F , as functions of $1/k_F a$, for the three distributions (a) $|\phi_{\text{BCS}}(r)|^2$, (b) $G_{\uparrow\downarrow}(r)$, and (c) $G_{\uparrow\uparrow}(r)$. Solid lines correspond to the exponential decay lengths (a) χ_{BCS} , (b) $\chi_{\uparrow\downarrow}$, (c) $\chi_{\uparrow\uparrow}$. Large dashed lines correspond to χ_b in the three panels. Short dashed lines are the average pair radius (a) ξ_{BCS} and the correlation lengths (b) $\xi_{\uparrow\downarrow}$ and (c) $\xi_{\uparrow\uparrow}$, as described in Sec. III. For comparison we show a few points extracted from calculations already reported. The points in panel (a) are of ξ_{BCS} from Ref. [27] and those in panel (b) are of $\xi_{\uparrow\downarrow}$ from Ref. [38].

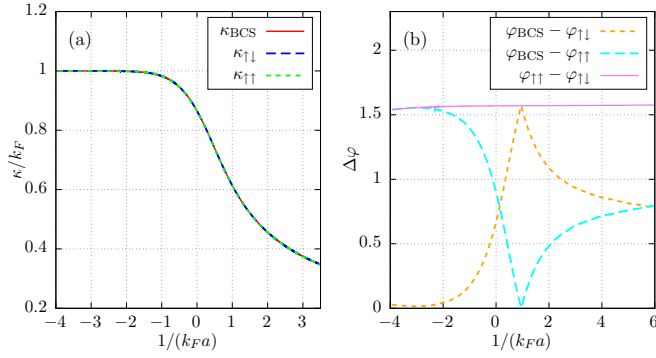


FIG. 4. (a) Characteristic wave vectors κ_{BCS} , $\kappa_{\uparrow\downarrow}$, and $\kappa_{\uparrow\uparrow}$, scaled with k_F , and (b) phase differences $\varphi_{\text{BCS}} - \varphi_{\uparrow\downarrow}$, $\varphi_{\text{BCS}} - \varphi_{\uparrow\uparrow}$, and $\varphi_{\uparrow\downarrow} - \varphi_{\uparrow\uparrow}$, in the long-distance behavior of the respective BCS pair probability distributions and the density correlation functions; see Fig. 2.

density correlations, since there must be a spatial correlation of the spin species due to pairing. In the BCS limit the characteristic wave number approaches the Fermi momentum k_F , an expected result [26,37], yet for the BEC limit it appears to slowly vanish. The latter seems to be in agreement with the fact that, in such a limit, the $\uparrow\downarrow$ atoms form molecules and the gas should appear completely uncorrelated for large distances, as in any common gas. However, by looking at Fig. 4(b), where the phase differences are shown, $\varphi_{\uparrow\downarrow} - \varphi_{\uparrow\uparrow}$ and $\varphi_{\text{BCS}} - \varphi_{\uparrow\downarrow}$, we observe that the former is always π while the latter changes as a function of $1/k_F a$. The former perfect phase difference can already be observed at short distances in the upper panel of Fig. 2(a). Thus, the correlation functions $G_{\uparrow\downarrow}(r)$ and $G_{\uparrow\uparrow}(r)$ show a very deep structure not only of the $\uparrow\downarrow$ pairs but also of the whole gas mixture, particularly in the BCS side: as $1/k_F a \rightarrow -\infty$, the exponential decay lengths χ_α and the correlation lengths ξ_α (see the following

section) for both correlation functions diverge in the same way, indicating that those quantities become irrelevant in determining the structure. Hence, the equality of $\kappa_{\uparrow\downarrow} = \kappa_{\uparrow\uparrow}$ and the constancy of the phase difference $\varphi_{\uparrow\uparrow} - \varphi_{\uparrow\downarrow}$, indicate an average alternating shell structure from the perspective of any given atom. Although this structure remains on the BEC side, it is severely diminished by the vanishing of both $\chi_{\uparrow\downarrow}$ and $\chi_{\uparrow\uparrow}$.

IV. MEAN PAIR RADIUS AND CORRELATION LENGTHS

Although all the spatial information we seek is in principle contained in the full distribution functions described in the previous section, there is a very important associated single quantity that serves to characterize their overall behavior. This is the second moment of the given spatial distribution, which in the case of the BCS pair probability distribution function yields the mean pair radius and in the correlation functions gives their corresponding correlation lengths. These are defined as follows:

$$\xi_\alpha^2 = \frac{|\int r^2 \rho_\alpha(r) d^3 r|}{|\int \rho_\alpha(r) d^3 r|}, \quad (24)$$

where $\rho_\alpha(r)$ is, again, either the BCS pair probability density distribution $|\phi_{\text{BCS}}(r)|^2$, the pair correlation function $G_{\uparrow\downarrow}(r)$, or the same spin-correlation function $G_{\uparrow\uparrow}(r)$. In the Appendix we provide details for the calculation of the different lengths ξ_α . Similarly to the procedure used to obtain Eqs. (12), (14), and (16), one can also find closed analytical expressions for the corresponding lengths in terms of hypergeometric functions. In the case of the $\uparrow\downarrow$ and $\uparrow\uparrow$ correlation lengths, the final result can be written explicitly as simple algebraic functions.

We quote here the analytical expressions for the average pair radius ξ_{BCS} and the correlation lengths $\xi_{\uparrow\downarrow}$ and $\xi_{\uparrow\uparrow}$:

$$\xi_{\text{BCS}}^2 = \frac{\hbar^2}{m(\mu^2 + \Delta^2)^{1/2}} \left\{ \frac{1}{\sqrt{2}(1-z)(1+z)^{1/2}} \frac{1 + 2z - z^2 - 2z^3 + 2\sqrt{2}(1+z)^{1/2}(P_{\frac{5}{2}}(z) - zP_{\frac{3}{2}}(z))}{-F(\frac{7}{2}, -\frac{5}{2}; 2, \frac{1-z}{2}) + zF(\frac{5}{2}, -\frac{3}{2}; 2, \frac{1-z}{2})} \right\}, \quad (25)$$

$$\xi_{\uparrow\downarrow}^2 = \frac{1}{8} \frac{\hbar^2}{2m(\mu^2 + \Delta^2)^{1/2}} \frac{1}{(1+z)^2} \frac{5 + 8z + 3z^2}{(1+z)^2}, \quad (26)$$

$$\xi_{\uparrow\uparrow}^2 = \frac{3}{8} \frac{\hbar^2}{2m(\mu^2 + \Delta^2)^{1/2}} \left(\frac{1-z}{1+z} \right). \quad (27)$$

In Figs. 3(a)–3(c), we plot ξ_{BCS} , $\xi_{\uparrow\downarrow}$, and $\xi_{\uparrow\uparrow}$, respectively, as functions of $1/k_F a$ with short dashed lines. Their asymptotic limits, including that of the binding-energy pair distribution, in the BCS limit, $z \rightarrow -1$ and $1/k_F a \rightarrow -\infty$, are

$$\begin{aligned} \xi_{\text{BCS}} &\approx \frac{\sqrt{105}}{2k_F} \left[\psi\left(\frac{7}{2}\right) - \psi\left(\frac{5}{2}\right) \right]^{1/2} = \sqrt{\frac{21}{2}} \frac{1}{k_F}, \\ \xi_{\uparrow\downarrow} &\approx \frac{1}{\sqrt{2}} \frac{e^2}{8k_F} e^{-\frac{\pi}{2k_F a}}, \quad \xi_{\uparrow\uparrow} \approx \sqrt{\frac{3}{2}} \frac{e^2}{8k_F} e^{-\frac{\pi}{2k_F a}}, \\ \xi_b &\approx \frac{2}{\sqrt{3}} \frac{e^2}{8k_F} e^{-\frac{\pi}{2k_F a}}, \end{aligned} \quad (28)$$

where $\psi(x)$ is the digamma function. Note that, in the BCS limit, ξ_{BCS} reaches a finite limit. A few points extracted from the results reported in Refs. [27] and [38] are plotted in Fig. 3, showing agreement with our analytic results. Thus, while $|\phi_{\text{BCS}}(r)|^2$ does become long ranged in the limit, we recall that χ_{BCS} appears to bend in the BCS limit, see Fig. 3(a), growing slower than $\chi_{\uparrow\downarrow}$ and $\chi_{\uparrow\uparrow}$. As a consequence, the numerator and denominator of Eq. (24) both diverge as $\sim \Delta^{-1}$, yielding a finite ξ_{BCS} . Thus, from the perspective of the pair wave function, the pair size reaches a finite value in the BCS limit. This is in stark contrast with the density correlation lengths $\xi_{\uparrow\downarrow}$ and $\xi_{\uparrow\uparrow}$, which indeed diverge. However, there is no contradiction since the latter are correlation lengths and their

divergence are in agreement with the expected notion that the correlation functions become long range. This indicates that, while average pair radius is finite, the algebraic decay of the wave function allows for pairs of all sizes. We also note that, up to numerical factors of order one, $\xi_{\uparrow\downarrow} \approx \xi_{\uparrow\uparrow} \approx \xi_b \sim \Delta^{-1}$, also expressing the known fact that the gap is the relevant energy scale in the BCS limit [25], which agrees with the Pippard coherence length [15].

In the BEC limit, $z \rightarrow +1$ and $1/k_F a \rightarrow +\infty$, we now have the asymptotic behavior,

$$\begin{aligned} \xi_{\text{BCS}} &\approx \frac{a}{\sqrt{2}}, & \xi_{\uparrow\downarrow} &\approx \frac{a}{\sqrt{2}}, \\ \xi_{\uparrow\uparrow} &\approx \sqrt{\frac{1}{2\pi}}(k_F a)^{3/2}a, & \xi_b &\approx \frac{a}{\sqrt{2}}. \end{aligned} \quad (29)$$

While now $\xi_{\text{BCS}} \approx \xi_{\uparrow\downarrow} \approx \xi_b \sim a \sim |\mu|^{-1/2}$, showing that the relevant energy is μ and no longer the gap, the different behavior is shown by $\xi_{\uparrow\uparrow}$ which vanishes much faster than the others, as can be seen in Fig. 3(c). This can be interpreted as the loss of fermionic correlation between $\uparrow\uparrow$ and $\downarrow\downarrow$ atoms, since they now are part of bosonic indistinguishable molecules. This is in line with the attained BEC character of the gas in such a limit. To reinforce this point, the decorrelation observed in the BEC side is accompanied by the vanishing of the characteristic wave vectors $\kappa_{\uparrow\downarrow}$ and $\kappa_{\uparrow\uparrow}$; namely, the wavelength of the nested structure gets diluted as the pairs become tighter.

We point out that $g_{\uparrow\downarrow}(r)$, the Fourier transform of $u_k v_k$, see Eq. (15), and whose square yields the pair correlation function $G_{\uparrow\downarrow}(r)$, has also been identified as the ‘‘pair wave function’’ because it obeys a Schrödinger-like equation, as can be obtained from the gap equation (5) [16,23,25]. In this regard, it is considered that $g_{\uparrow\downarrow}(\mathbf{r})$ and its associated correlation length $\xi_{\uparrow\downarrow}$ essentially bears the Cooper pair structure. Indeed, Strinati and collaborators [15,16,29,38] have thoroughly studied this function and its length not only in the zero-temperature limit as here but also at finite temperatures, and one can also mention results of this function for finite range potentials [30,40,41]. It is thus of interest to point out that the correlation function $G_{\uparrow\downarrow}(r)$, apart from its spatial oscillations, is the one most closely related to the binding-energy wave function along the whole crossover. As we have studied here, however, the full structure of the mixture emerges not only when the $\uparrow\downarrow$ correlation function is considered but also when the $\uparrow\uparrow$ correlation function and the BCS-pair probability distributions are taken into account.

V. CONCLUSIONS AND DISCUSSIONS

In this article we have addressed the spatial structure of the gas mixture of two different fermionic species throughout the BEC-BCS crossover at the zero-temperature mean-field level. We analyze the BCS pair probability distribution function that enters the many-body BCS ansatz and the equal $\uparrow\uparrow$ and pair $\uparrow\downarrow$ density correlation functions. By exploiting their nonanalytic structure in the complex plane of the Fourier \mathbf{k} space, we are able to accurately calculate them. In this way, we can access their long-distance properties, such as their exponential

decay length, oscillatory behavior, and relative phases, see Fig. 2, that determine their physical asymptotic behavior, which is crucial to the understanding and characterization of the different regimes along the crossover. The technique developed here should be useful for dealing with typical integrals that appear in related problems, since it avoids the numerical difficulties of Fourier transforms of algebraic decaying functions. This technical achievement was not only responsible for our main physical results but we believe it is the way to calculate many of the integrals that appear, for instance, in calculations that include finite temperature and fluctuations.

To summarize, as shown in Fig. 3, we find that, while the three exponential decay lengths behave similarly, the corresponding correlation lengths do show different behavior, indicating the different physical properties that each distribution addresses. In Fig. 4, we observe that the spatial oscillating frequencies of the three functions are the same, which with the relative phase-difference behavior, point out the emergence of a nested spatial structure of atoms with parallel and antiparallel spins, on average. This structure can, in principle, be experimentally tested [25,39]. The exponential decay length and frequency oscillations correspond to features of two-body physics, already estimated in the BCS and BEC limit, with our work contributing to their full description along the whole crossover. In addition, we have also provided an analytic systematic procedure to deal with the integrals appearing in the thermodynamic quantities and in the calculation of correlation lengths. We have verified that some of our expressions indeed agree with those already reported [27,38].

There are, however, natural extensions of this study that should be addressed. One is the consideration of realistic interatomic finite-range potentials [40,41] and the other is the inclusion of finite temperatures [38] still at the level of a mean-field description. For the case of finite temperatures there are already solid advances, especially for the $\uparrow\downarrow$ correlation function [16,38]. In this context there is an additional length, the *phase* length, which is associated with the Gaussian fluctuations of the order parameter [29]. Although such an analysis is beyond the scope of the present work, it is of interest to point out that such a quantity diverges in both limits, as Δ^{-1} in the BCS limit and as $|\mu|^{1/2}$ in the BEC limit, taking its smallest value near unitarity, in contrast with the lengths discussed here. This suggests, as a natural continuation of the present work, to look at the fluctuations of all distributions here studied, even at the Gaussian level.

Our calculations can be contrasted with those used in Monte Carlo methods. The structure of the correlators that we found may contribute to give physical insight for new variational functions [36]. Also, comparing with those Monte Carlo calculations, it can be seen that the correlation lengths obtained here are a lower bound of the correlation lengths of the complete many-body Hamiltonian [26].

To conclude we would like to briefly address the consequences of the long-range behavior near unitarity and in the BCS limit on current experimental studies with confined ultracold gases. Typically, specially in the BEC side [7,42,43] and in gases with bosons such as ^{87}Rb [44] and ^7Li , [45], the local density approximation has been shown to be quite accurate.

This can be understood as a result that the density correlation length is (much) smaller than the size of the system. However, this may not be true in the near and deep BCS regions. That is, those vapor clouds may still be of relative mesoscopic size and, therefore, the usual thermodynamic description could not be directly applied to them. This deserves a further and careful analysis of the different length scales involved in those experiments.

ACKNOWLEDGMENTS

We are grateful for support from grants CONACYT 255573 and UNAM PAPIIT-IN105217. J.C.O.-J. acknowledges support from a CONACYT scholarship.

APPENDIX: ANALYTICAL EXPRESSIONS AND CONTOUR DEFORMATION

1. Analytical expressions for thermodynamic functions and correlation lengths

In expressions (5)–(7), for the gap, number density, and energy, the difficulty of the \mathbf{k} integrals lie in the handling of the factor $[(\epsilon_k - \mu)^2 + \Delta^2]^\beta$, when $\beta = -3/2, -1/2, 1/2, \dots$, a positive or negative semi-integer. The suggestion is to make the following change of variables and rearrangements [46]:

$$\begin{aligned} & [(\epsilon_k - \mu)^2 + \Delta^2]^\beta \\ &= (\mu^2 + \Delta^2)^\beta (x^2 + 2xz + 1)^\beta \\ &= (\mu^2 + \Delta^2)^\beta (1+x)^{2\beta} \left(1 - \frac{2(1-z)x}{(1+x)^2}\right)^\beta, \end{aligned} \quad (\text{A1})$$

where $x = \epsilon_k/(\mu^2 + \Delta^2)^{1/2}$ and $z = -\mu/(\mu^2 + \Delta^2)^{1/2}$ and integrate over x . Since $x/(1+x)^2 < 1$ for $x \rightarrow 0$ and $x \rightarrow \infty$, one can perform a series expansion in powers of $2(1-z)x/(1+x)^2$ of expression (A1). Then, all the resulting integrals can be rearranged as factors of a power series in $(1-z)/2$ that can be integrated term by term. This can be a lengthy exercise but it yields a series of convergent integrals, which are all beta functions. The resulting series can be cast in terms of hypergeometric functions,

$$F\left(a, b; c, \frac{1-z}{2}\right) = \sum_{n=0}^{\infty} \frac{(a)_n (b)_n}{n! (c)_n} \left(\frac{1-z}{2}\right)^n, \quad (\text{A2})$$

where $(d)_n$ are Pochhammer symbols. Depending on a, b , and c , in some cases the hypergeometric functions can be written in terms of Legendre functions and in others they can be written explicitly [46,47].

For the calculation of the lengths ξ_α , Eq. (24), we first write the distribution $\rho(\mathbf{r})$ in terms of its Fourier expression. For instance, for $\rho_{\text{BCS}}(r) = |\phi_{\text{BCS}}(r)|^2$, the length ξ can be recast as

$$\begin{aligned} \xi_{\text{BCS}}^2 &= \frac{\int r^2 |\phi_{\text{BCS}}(r)|^2 d^3r}{\int |\phi_{\text{BCS}}(r)|^2 d^3r} \\ &= \frac{\int |\nabla_k \tilde{\phi}_{\text{BCS}}(k)|^2 d^3k}{\int |\tilde{\phi}_{\text{BCS}}(k)|^2 d^3k}, \end{aligned} \quad (\text{A3})$$

where $\tilde{\phi}_{\text{BCS}}(k) = v_k/u_k$ is the Fourier transform of $\phi_{\text{BCS}}(r)$. One integrates the expression in the second line by using the

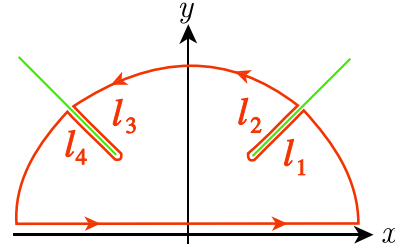


FIG. 5. Illustration of the contour used in the Cauchy integral formula, with $\kappa = x + iy$. Surrounding the branch cuts give four paths denoted by l_i , with $i = 1, 2, 3, 4$.

procedure described in the previous paragraph (similarly for $\xi_{\uparrow\downarrow}$ and $\xi_{\uparrow\uparrow}$).

2. Contour deformation for the calculation of integral Eq. (19)

Here we show the steps to make the contour integration around the branch cuts in Eq. (19). In the following, we use the pair wave function v_k/u_k , but the same procedure can be used for $u_k v_k$ and v_k^2 .

Using the gap $\Delta = \hbar^2 k_\Delta^2 / 2m$ to adimensionalize the k integral and defining $\mu_\Delta = \mu/\Delta$, the pair wave function is given by the following equation:

$$(k_\Delta r) \phi(k_\Delta r) = \frac{k_\Delta^3}{4\pi^2 i} I(k_\Delta r), \quad (\text{A4})$$

where we have arranged the equation to focus only in the following integral:

$$I(k_\Delta r) = \int_{-\infty}^{\infty} \kappa [\sqrt{(\kappa^2 - \mu_\Delta)^2 + 1} - (\kappa^2 - \mu_\Delta)] e^{i\kappa(k_\Delta r)} d\kappa. \quad (\text{A5})$$

The integrand has four branch cuts due to the square root, as illustrated in Fig. 5. To calculate them we use the principal branch of the complex logarithm function. Then, the points κ in the complex plane belonging to the branch cuts satisfy the following equations:

$$\text{Re}[(\kappa^2 - \mu_\Delta)^2 + 1] \leq 0, \text{ and } \text{Im}[(\kappa^2 - \mu_\Delta)^2 + 1] = 0. \quad (\text{A6})$$

Using $\kappa = x + iy$ it can be shown that the branch cuts correspond to points in the hyperbola $x^2 - y^2 = \mu_\Delta$ with their magnitude satisfying $|\kappa|^2 \geq (\mu_\Delta^2 + 1)^{1/2}$. Then, choosing a contour \mathcal{C} which surrounds the branch cuts in the upper half plane like the one shown in Fig. 5, the Cauchy theorem allows us to conclude that $\oint_{\mathcal{C}} f(\kappa) d\kappa = 0$, where

$$f(\kappa) = \kappa \sqrt{(\kappa^2 - \mu_\Delta)^2 + 1} e^{i\kappa(k_\Delta r)}. \quad (\text{A7})$$

The term $\kappa(\kappa^2 - \mu_\Delta) e^{i\kappa(k_\Delta r)}$ can be removed from the integrand because it is analytic everywhere. Hence, it can be

concluded that

$$\int_{-\infty}^{\infty} f(\kappa) d\kappa = 2 \int_{l_2}^{\infty} \kappa i \sqrt{(\kappa^2 - \mu_{\Delta})^2 + 1} |e^{i\kappa(k_{\Delta}r)} d\kappa + 2 \int_{l_4}^{\infty} \kappa i \sqrt{(\kappa^2 - \mu_{\Delta})^2 + 1} |e^{i\kappa(k_{\Delta}r)} d\kappa. \quad (\text{A8})$$

with the branch cuts parametrized by $\gamma_2(t) = t + i(t^2 - \mu_{\Delta})^{1/2}$ and $\gamma_4(t) = -t + i(t^2 - \mu_{\Delta})^{1/2}$, with $t \in [t_0, \infty)$ and

$$t_0 = \left(\frac{\mu_{\Delta} + (\mu_{\Delta}^2 + 1)^{1/2}}{2} \right)^{1/2}. \quad (\text{A9})$$

Substitution of the parametric equations into Eq. (A8) and identifying the integral $I(k_{\Delta}r)$ with the integral of $f(\kappa)$ in the reals we arrive at the desired result,

$$I(k_{\Delta}r) = -4i \int_{t_0}^{\infty} \left(\frac{2t^2 - \mu_{\Delta}}{\sqrt{t^2 - \mu_{\Delta}}} \right) \sqrt{4t^2(t^2 - \mu_{\Delta}) - 1} \times \exp[-\sqrt{t^2 - \mu_{\Delta}}(k_{\Delta}r)] \sin [t(k_{\Delta}r)] dt, \quad (\text{A10})$$

which by a change of dimensions of k_{Δ} in favor of k_F , yields Eq. (20).

-
- [1] B. Mukherjee, Z. Yan, P. B. Patel, Z. Hadzibabic, T. Yefsah, J. Struck, and M. W. Zwierlein, *Phys. Rev. Lett.* **118**, 123401 (2017).
- [2] M. W. Zwierlein, C. A. Stan, C. H. Schunck, S. M. F. Raupach, A. J. Kerman, and W. Ketterle, *Phys. Rev. Lett.* **92**, 120403 (2004).
- [3] C. A. Regal, M. Greiner, and D. S. Jin, *Phys. Rev. Lett.* **92**, 040403 (2004).
- [4] J. Kinast, S. L. Hemmer, M. E. Gehm, A. Turlapov, and J. E. Thomas, *Phys. Rev. Lett.* **92**, 150402 (2004).
- [5] T. Bourdel, L. Khaykovich, J. Cubizolles, J. Zhang, F. Chevy, M. Teichmann, L. Tarruell, S. J. J. M. F. Kokkelmans, and C. Salomon, *Phys. Rev. Lett.* **93**, 050401 (2004).
- [6] C. Chin, M. Bartenstein, A. Altmeyer, S. Riedl, S. Jochim, J. H. Denschlag, and R. Grimm, *Science* **305**, 1128 (2004).
- [7] J. H. V. Nguyen, M. C. Tsatsos, D. Luo, A. U. J. Lode, G. D. Telles, V. S. Bagnato, and R. G. Hulet, *Phys. Rev. X* **9**, 011052 (2019).
- [8] M. J. H. Ku, W. Ji, B. Mukherjee, E. Guardado-Sanchez, L. W. Cheuk, T. Yefsah, and M. W. Zwierlein, *Phys. Rev. Lett.* **113**, 065301 (2014).
- [9] D. Husmann, S. Uchino, S. Krinner, M. Lebrat, T. Giamarchi, T. Esslinger, and J.-P. Brantut, *Science* **350**, 1498 (2015).
- [10] G. Valtolina, A. Burchianti, A. Amico, E. Neri, K. Xhani, J. A. Seman, A. Trombettoni, A. Smerzi, M. Zaccanti, M. Inguscio, and G. Roati, *Science* **350**, 1505 (2015).
- [11] M. Randeria, J.-M. Duan, and L.-Y. Shieh, *Phys. Rev. Lett.* **62**, 981 (1989).
- [12] R. Micnas, J. Ranninger, and S. Robaszkiewicz, *Rev. Mod. Phys.* **62**, 113 (1990).
- [13] M. Drechsler and W. Zwerger, *Ann. Phys. (Berlin, Ger.)* **504**, 15 (1992).
- [14] R. Haussmann, *Z. Phys. B: Condens. Matter* **91**, 291 (1993).
- [15] F. Pistolesi and G. C. Strinati, *Phys. Rev. B* **49**, 6356 (1994).
- [16] G. C. Strinati, P. Pieri, G. Röpke, P. Schuck, and M. Urban, *Phys. Rep.* **738**, 1 (2018).
- [17] G. A. Baker, *Phys. Rev. C* **60**, 054311 (1999).
- [18] U. Lombardo, P. Nozières, P. Schuck, H.-J. Schulze, and A. Sedrakian, *Phys. Rev. C* **64**, 064314 (2001).
- [19] N. Andrenacci, A. Perali, P. Pieri, and G. C. Strinati, *Phys. Rev. B* **60**, 12410 (1999).
- [20] M. Jin, M. Urban, and P. Schuck, *Phys. Rev. C* **82**, 024911 (2010).
- [21] J. Blatt, *Theory of Superconductivity* (Academic Press, New York, 1964).
- [22] D. M. Eagles, *Phys. Rev.* **186**, 456 (1969).
- [23] A. J. Leggett, in *Modern Trends in the Theory of Condensed Matter* (Springer, Berlin, Heidelberg, 1980), pp. 13–27.
- [24] P. Nozières and S. Schmitt-Rink, *J. Low Temp. Phys.* **59**, 195 (1985).
- [25] W. Ketterle and M. W. Zwierlein, *Riv. Nuovo Cimento* **164**, 95 (2008).
- [26] S. Giorgini, L. P. Pitaevskii, and S. Stringari, *Rev. Mod. Phys.* **80**, 1215 (2008).
- [27] G. Ortiz and J. Dukelsky, *Phys. Rev. A* **72**, 043611 (2005).
- [28] T. Papenbrock and G. F. Bertsch, *Phys. Rev. C* **59**, 2052 (1999).
- [29] M. Marini, F. Pistolesi, and G. Strinati, *Eur. Phys. J. B* **1**, 151 (1998).
- [30] S. Musolino and M.-L. Chiofalo, *Eur. Phys. J. Spec. Top.* **226**, 2793 (2017).
- [31] J. R. Engelbrecht, M. Randeria, and C. A. R. Sáde Melo, *Phys. Rev. B* **55**, 15153 (1997).
- [32] M. Casas, J. M. Getino, M. de Llano, A. Puente, R. M. Quick, H. Rubio, and D. M. van der Walt, *Phys. Rev. B* **50**, 15945 (1994).
- [33] H. Bethe, R. Peierls, and D. R. Hartree, *Proc. R. Soc. London, Ser. A* **148**, 146 (1935).
- [34] J. Bardeen, L. N. Cooper, and J. R. Schrieffer, *Phys. Rev.* **108**, 1175 (1957).
- [35] M. Tinkham, *Introduction to Superconductivity*, Dover Books on Physics Series (Dover Publications, New York, 2004).
- [36] R. Pessoa, S. Gandolfi, S. A. Vitiello, and K. E. Schmidt, *Phys. Rev. A* **92**, 063625 (2015).
- [37] L. Landau and E. Lifshitz, *Statistical Physics II* (Elsevier Science, 2013), Vol. 5.
- [38] F. Palestini and G. C. Strinati, *Phys. Rev. B* **89**, 224508 (2014).
- [39] C. H. Schunck, Y.-i. Shin, A. Schirotzek, and W. Ketterle, *Nature (London)* **454**, 739 (2008).
- [40] S. Caballero-Benitez, R. Paredes, and V. Romero-Rochin, *Phys. Lett. A* **377**, 1756 (2013).
- [41] E. Neri, S. Caballero-Benitez, V. Romero-Rochin, and R. Paredes, *Phys. Scr.* **95**, 034013 (2020).

- [42] T.-L. Ho and Q. Zhou, *Nat. Phys.* **6**, 131 (2009).
- [43] S. Nascimbène, N. Navon, F. Chevy, and C. Salomon, *New J. Phys.* **12**, 103026 (2010).
- [44] R. F. Shiozaki, G. D. Telles, P. Castilho, F. J. Poveda-Cuevas, S. R. Muniz, G. Roati, V. Romero-Rochin, and V. S. Bagnato, *Phys. Rev. A* **90**, 043640 (2014).
- [45] N. Navon, S. Piatecki, K. Günter, B. Rem, T. C. Nguyen, F. Chevy, W. Krauth, and C. Salomon, *Phys. Rev. Lett.* **107**, 135301 (2011).
- [46] H. Bateman, *Higher Transcendental Functions* (McGraw-Hill Book Company, Inc., 1953), Vol. I.
- [47] S. Wolfram, Legendre, <https://reference.wolfram.com/language/ref/LegendreP.html> (2019).